Rotational Effects on the Overtone-Induced Isomerization Rate for $CHD_2NC \rightarrow CHD_2CN$

J. H. Gutow[1] and R. N. Zare*

Department of Chemistry, Stanford University, Stanford, California 94305-5080 *(Received: August 15, 1991; In Final Form: November 14, 1991)*

CHD_2NC reactant was prepared in a few rotational states, with approximately 1.7 kcal/mol of excess vibrational energy above the barrier to isomerization, by excitation of well-resolved $^{\Delta K}Q$ bandheads of the 5-0 C-H overtone spectrum. Experiments were performed in a static gas cell using IR absorption to monitor the progress of the reaction and a Stern-Volmer analysis to determine the rate constants. The isomerization rate constants were found to decrease significantly as the K quantum number of the excited reactants increased. Rice-Ramsperger-Kassel-Marcus calculations including angular momentum effects have been used in an attempt to simulate the observed isomerization rate constants over the small energy range of this study. Calculations using either conservation or nonconservation of the K quantum number cannot qualitatively reproduce the observed decrease in rate constant with increasing K. We are unable to establish the origin of this discrepancy.

I. Introduction

Unimolecular reactions provide the basis for much of our detailed understanding of kinetics. Statistical theories, such as the Rice-Ramsperger-Kassel-Marcus (RRKM) theory[2-4] and statistical adiabatic channel models (SACM),[5-7] have successfully described such processes. One facet of these theories not well tested experimentally is the effect of rotational excitation of the reactant on the reaction rate. Yet considerable theoretical work has shown the importance of angular momentum conservation and rotational energy in unimolecular reactions.[5,6,8-11]

This paper describes the experimental observation of rotational-state-dependent isomerization rate constants for the reaction

$$CHD_2NC + h\nu \rightarrow CHD_2CN$$

Using the 5-0 C-H vibrational overtone, the reactant is prepared in a few rotational states, with approximately 1.7 kcal/mol of excess vibrational energy above the barrier to isomerization. The CHD_2NC 5-0 overtone spectrum exhibits well-resolved $^{\Delta K}Q$ bandheads, which allow selection of the K state of the excited molecules where K is the projection of the total rotational angular momentum J on the top axis.

Rabinovitch and co-workers[12-15] began thermal studies of this reaction (CH_3NC and CD_3NC) almost 30 years ago. They estimated the barrier height to be 38 kcal/mol. Because the reaction is approximately 24 kcal/mol exothermic, a statistical behavior would suggest that few if any of the products can re-cross the barrier to become reactants. These early studies also included careful RRKM analyses of the data and provided impetus for ab initio and trajectory studies.[10,16-18]

Reddy and Berry realized that the reactants could be prepared with a narrower energy distribution by vibrational overtone excitation than by thermal activation. They studied the isomerization of CH_3NC to CH_3CN and observed behavior consistent with RRKM theories but with significant discrepancies.[19,20] Subsequent calculations by Miller and Chandler,[21] modified to account for inefficient collisional deactivation, suggested these discrepancies may arise from the simple strong collider assumption used in Reddy and Berry's analysis as well as from a small error in the thermally determined barrier height. Trajectory calculations by Sumpter and Thompson[22] indicated that this isomerization process behaves statistically, although in their calculations energy redistribution in the molecule occurred in a mode-specific way that was highly dependent upon the details of the potential chosen.

The CH_3 overtones at room temperature are broad, unresolved features. They apparently consist of many overlapping transitions.[23] Thus, no rotational-state specificity was available in Reddy and Berry's experiments.

Snavely et al.[24] reported the most recent overtone-induced isomerization studies of CH_3NC. They determined the average energy transferred per collision for several buffer gases. For neat CH_3NC, they found this energy to be approximately 1000 cm^{-1} (~2.9 kcal/mol). Again their results appear consistent with RRKM theories.

CHD_2NC is an ideal system for studying rotational effects in a unimolecular reaction. Unlike its undeuterated analogue, this molecule exhibits resolved rotational structure in its high overtones. In addition, the rotationally resolved band in the region of the 5-0 C-H overtone transition is only approximately 1.7 kcal/mol above the barrier to reaction. State-dependent effects should be much more significant when close to the barrier to reaction than when high above it.

In the present work, we compare the observed rotational state dependence with predictions using standard RRKM theory including rotational effects.[2-4] The experiments were performed in a static gas cell using IR absorption to monitor the reaction's progress. A Stern-Volmer analysis was used to determine the

(1) Present address: Department of Chemistry, Columbia University, New York, NY 10027.
(2) Gilbert, R. G.; Smith, S. C. *Theory of Unimolecular and Recombination Reactions*; Blackwell Scientific Publications: Boston, 1990.
(3) Forst, W. *Theory of Unimolecular Reactions*; Academic Press: New York, 1973.
(4) Forst, W. *J. Chim. Phys. Phys.-Chim. Biol.* **1990**, *87*, 715.
(5) Troe, J. *An. Asoc. Quim. Argent.* **1985**, *73*, 63.
(6) Troe, J. *J. Chem. Phys.* **1983**, *79*, 6017.
(7) Quack, M.; Troe, J. *Ber. Bunsen-Ges. Phys. Chem.* **1974**, *78*, 240.
(8) Waage, E. V.; Rabinovitch, B. S. *Chem. Rev.* **1970**, *70*, 377.
(9) Miller, J. A.; Brown, N. J. *J. Phys. Chem.* **1982**, *86*, 772.
(10) Marks, A. J.; Murrell, J. N.; Stace, A. J. *Chem. Phys. Lett.* **1989**, *154*, 492.
(11) Troe, J. *J. Phys. Chem.* **1984**, *88*, 4375.
(12) Schneider, F. W.; Rabinovitch, B. S. *J. Am. Chem. Soc.* **1962**, *84*, 4215.
(13) Schneider, F. W.; Rabinovitch, B. S. *J. Am. Chem. Soc.* **1963**, *85*, 2365.
(14) Rabinovitch, B. S.; Gilderson, R. W.; Schneider, R. W. *J. Am. Chem. Soc.* **1965**, *87*, 158.
(15) Chan, S. C.; Rabinovitch, B. S.; Bryant, J. T.; Spicer, L. D.; Fujimoto, T.; Lin, Y. N.; Pavlou, S. P. *J. Phys. Chem.* **1970**, *74*, 3160.
(16) Liskow, D. H.; Bender, C. F.; Schaefer, H. F., III *J. Chem. Phys.* **1972**, *57*, 4509.
(17) Saxe, P.; Yamaguchi, Y.; Pulay, P.; Schaefer, H. F., III *J. Am. Chem. Soc.* **1980**, *102*, 3718.
(18) Ha, T.-K. *J. Mol. Stuct.* **1972**, *11*, 185.
(19) Reddy, K. V.; Berry, M. J. *Chem. Phys. Lett.* **1977**, *52*, 111.
(20) Reddy, K. V.; Berry, M. J. *Faraday Discuss. Chem. Soc.* **1979**, *67*, 188.
(21) Miller, J. A.; Chandler, D. W. *J. Chem. Phys.* **1986**, *85*, 4502.
(22) Sumpter, B. G.; Thompson, D. L. *J. Chem. Phys.* **1987**, *87*, 5809.
(23) Crofton, M. W.; Stevens, C. G.; Klenerman, D.; Gutow, J. H.; Zare, R. N. *J. Chem. Phys.* **1988**, *12*, 7100 and references therein.
(24) Snavely, D. L.; Zare, R. N.; Miller, J. A.; Chandler, D. W. *J. Phys. Chem.* **1986**, *90*, 3544.

0022-3654/92/2096-2534$03.00/0

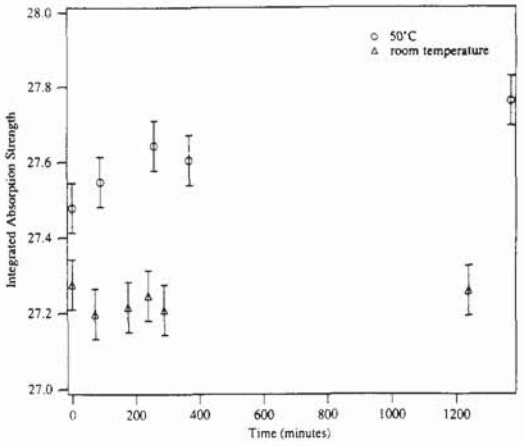

Figure 2. Integrated intensity of the N≡C stretching band of CHD_2NC versus time for a sample left sitting in the isomerization cell. The slight upward drift in the intensity for the 50 °C data is caused by an instability in the temperature control for the FTIR spectrometer. This instability was repaired.

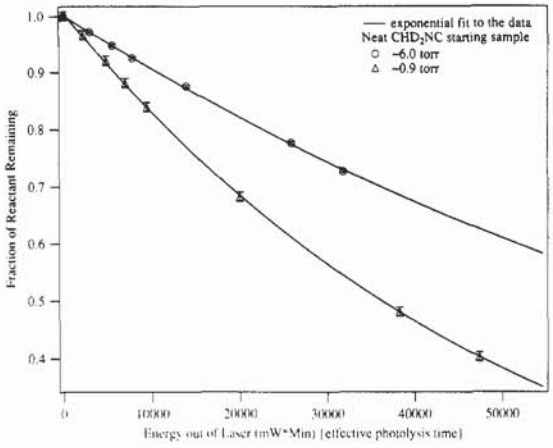

Figure 3. Effect of pressure on the observed reaction rate constants. The curves are single exponential fits to the data. The isomerization frequency was 13850.4 cm^{-1} ($^RQ_2$).

although the laser bandwidth is approximately 0.34 cm^{-1}, 0.5 cm^{-1} probably better represents the time-averaged excitation bandwidth. The laser power was monitored with an NRC 815 power meter and digitized at 0.2–1 Hz for future integration using a microcomputer (IBM PC) equipped with a 12-bit, analog-to-digital converter. The 0.1-Hz square-wave output of a Hewlett Packard function generator (Model 3300A) was digitized simultaneously on another channel to verify the time base. The sample cell was periodically removed from the dye laser, and an FTIR spectrum was taken of the sample using the IBM 98. This cycle was repeated until 20–60% of the sample was converted to CHD_2CN from CHD_2NC.

During a run, five to seven FTIR spectra were collected. A spectrum was taken roughly every 2 h for the first 8–10 h of photolysis. Subsequent spectra were taken at intervals varying between 3 and 9 h. A single run lasted about 30 h. Occasionally, at the end of a run, a gas chromatogram was taken of the gas sample to check for contamination and other products. The column was a Superox II 15- × 0.53-mm column (Alltech). The GC runs were programmed runs starting at 60 °C for 3 min followed by a ramp of 20 °C/min to 210 °C using He carrier gas at 10.4 mL/min. The isocyanide and cyanide retention times were approximately 2.1 and 3.4 min, respectively, but both had long tails. No other products were observed. We checked for background reactions by allowing samples to sit for one day without being photolyzed (see Figure 2).

1. Kinetics at Elevated Temperature. For the photolyses performed at 50 °C, the cell was mounted in the laser cavity using a form-fitted block of foam insulation. This insulating block was created by casting the cell into place with expanding foam insulation (Geocel Co.). The resulting block was cut into three pieces, a bottom and two top sections, so that the cell could be removed. The temperature was maintained to within 0.6 °C, using an Omega 9000 temperature controller with a type J thermocouple sensor, but the accuracy of the temperature is only ±2 °C. The cell was heated using about 12 V ac through 0.4-mm-diameter nichrome wire wrapped around the body of the cell in a spiral of approximately 0.5-cm spacing. The low voltage, which was slightly more than enough to maintain the desired temperature, prevented formation of hot spots in the cell, which might have caused a thermally induced background reaction. As shown in Figure 2, no significant background reaction occurred under these conditions, as indicated by the stability of the integrated N≡C stretch band intensity.

2. Laser Bandwidth Measurement. The bandwidth of the laser was measured using a piezo-scanned plane Fabry–Perot etalon (Spectra-Physics 581A) modified using plastic adaptors to hold 0.5-in.-diameter optics. The mirrors used were 95% reflective and were centered at 13793 cm^{-1} (725 nm) with antireflection coatings on their backsides (CVI Corp.). The FSR of the scanning etalon was measured by putting an additional thick, uncoated quartz etalon with a FSR of 0.934 cm^{-1} into the laser cavity and adjusting the laser to lase on two modes of this etalon. The major uncertainty in this calibration method was the measurement of the separation in volts between the modes on our oscilloscope. Once the wavenumbers scanned per volt were known, the voltage required to scan one FSR was measured. The scanning etalon was used at two mirror spacings, which gave FSRs of 6.5 ± 0.1 and 2.5 ± 0.04 cm^{-1}. Both configurations gave roughly the same laser bandwidth (0.34 ± 0.02 cm^{-1}), but for the 6.5-cm^{-1} FSR, the theoretical maximum resolution of the etalon would be only 0.1 cm^{-1},[29] which is barely adequate to measure a bandwidth of approximately 0.3 cm^{-1}. Based on measurements of the fwhm of the beating modes observed at the 2.5-cm^{-1} FSR, we estimate the finesse of the etalon to be between 35 and 40, when properly aligned. This finesse means the resolution is approximately 0.2 cm^{-1} for a FSR of 6.5 cm^{-1} and is 0.07 cm^{-1} or somewhat better for a FSR of 2.5 cm^{-1}. We believe that the resolution at the smaller FSR was adequate for this measurement because we observed the multiple laser modes within the laser bandwidth profile.

3. End Mirror Transmission Measurement. One check of the validity of the kinetics analysis is to calculate spectroscopic absorption cross sections from the data. To do this check, the relative intracavity laser power must be known. Because the laser power was monitored through the end mirror of the laser cavity, the transmission coefficient of the end mirror is needed to calculate the intracavity power. The transmission coefficient was measured at various laser frequencies using the laser as the light source for a home-built dual-beam spectrometer, which had a photodiode detector and an Hewlett Packard 8540A diode array spectrometer, with a resolution of approximately 38 cm^{-1}. We estimate that the fractional transmission coefficient for the mirror used in this experiment was (5.1 ± 0.3) × 10^{-4} over the frequency range of the experiment, where the uncertainty represents the range of values measured.

D. Vibrational Overtone Spectroscopy. The laser photoacoustic apparatus used to record the 5–0 C–H vibrational overtone spectra of CHD_2NC has been described previously.[30] The sample consisted of approximately 10 Torr of CHD_2NC buffered in approximately 300 Torr of Xe. The spectroscopic assignments and analysis will be detailed elsewhere.[31]

III. Data Analysis

A. Stern–Volmer Analysis. The raw data from a run consisted of a series of five to seven FTIR spectra of the contents of the

(29) Demtröder, W. *Laser Spectroscopy*; Springer-Verlag: New York, 1982.
(30) Davidsson, J.; Gutow, J. H.; Zare, R. N. *J. Phys. Chem.* **1990**, *94*, 4069.
(31) Gutow, J. H.; Hollenstein, H.; Quack, M. Manuscript in preparation.

TABLE I: Relative Isomerization Rate Constants (k) Corrected for the Laser Power and Absorption Cross Sections. All Constants Are Normalized to the $^RQ_0$ Transition

final K	transition	E, cm^{-1}	k 298 K	k 323 K	fractional change $((k_{323} - k_{298})/k_{298})$
4	$^PQ_5$	13809.3	0.78 ± 0.03		
3	$^PQ_4$	13815.4	0.95 ± 0.04	1.21 ± 0.08	0.27 ± 0.02
0	$^PQ_1$[a]	13833.6	0.85 ± 0.03		
?	^QQ[a]	13835.9	1.20 ± 0.05		
1	$^RQ_0$	13839.3	1.00 ± 0.05	1.41 ± 0.09	0.41 ± 0.03
2	$^RQ_1$	13845.1	0.81 ± 0.02	1.19 ± 0.06	0.47 ● 0.03
3	$^RQ_2$	13850.4	0.41 ± 0.01		

[a] These two bandheads overlap. The assignment is only approximate.

photolysis cell along with digitized traces of the laser output power. The integrated cross section for the N≡C absorption band was plotted versus the time-integrated laser output power, to yield a single exponential decay. The observed decay rate depends upon the starting pressure of CHD_2NC. At higher pressures, the decay rate decreases because the higher collision rate deactivates more of the excited molecules (see Figure 3). The decay rate was interpreted using a Stern–Volmer analysis and a kinetic model for overtone-induced isomerization of CH_3NC, suggested by Reddy and Berry.[19,20] The approximate expression for the expected rate constant, derived from a Taylor expansion of the solution, is

$$k_{app}(\nu) \approx \frac{-k_{iso}(\nu)k_a(\nu)[h\nu]}{k_{iso}(\nu) + k_d(\nu)[M] + k_a(\nu)[h\nu]} \quad (1)$$

Here ν is the photolysis frequency, $k_{app}(\nu)$ is the observed first-order decay rate constant, $k_a(\nu)$ is the rate constant for excitation of molecules by the laser (proportional to the absorption cross section), $k_{iso}(\nu)$ is the rate constant for isomerization of excited molecules in the absence of collisions, $[h\nu]$ is the concentration of photons (proportional to the laser power), $k_d(\nu)$ is the deactivation rate constant, which describes the rate at which molecules lose sufficient energy through collisions to make them unreactive, and [M] is the concentration of gas in the sample cell (proportional to the pressure).

The Stern–Volmer analysis consists of noting that $1/k_{app}(\nu)$ is linearly proportional to the collider density, [M]:

$$\frac{1}{-k_{app}(\nu)} \approx \frac{1}{k_{iso}(\nu)} + \frac{1}{k_a(\nu)[h\nu]} + \frac{k_d(\nu)}{k_{iso}(\nu)k_a(\nu)[h\nu]}[M] \quad (2)$$

The sum of the first two terms in this expression is the zero-pressure intercept. Since $k_{iso}(\nu) \approx 10^8\ s^{-1}$, the first term is negligible; hence the intercept is the second term, the inverse of the excitation rate ($k_a(\nu)[h\nu] \approx 10^{-5}\ s^{-1}$). Dividing expression 2 by the intercept yields an expression for a line with a slope that is proportional to the ratio of the collisional deactivation rate constant divided by the reaction (isomerization) rate constant (see Figure 4):

$$\frac{-k_a(\nu)[h\nu]}{k_{app}(\nu)} \approx 1 + \frac{k_d(\nu)}{k_{iso}(\nu)}[M] \quad (3)$$

The value of $k_{iso}(\nu)/k_d(\nu)$ (1/slope) normalized to $k_{iso}(\nu)/k_d(\nu)$ at 13839.3 cm^{-1} ($^RQ_0$) is the value reported in this work (see Figure 5 and Table I). Variations in this value reflect changes in $k_{iso}(\nu)$ or $k_d(\nu)$. The deactivation rate constant, $k_d(\nu)$, however, is expected to change little under the conditions of this experiment[19] (see the discussion below).

B. Error Analysis and Propagation. All errors reported in this work represent 95% confidence levels ($\pm 2\sigma$). The errors were propagated from the estimated errors in measuring the N≡C stretch cross section using the covariance matrix generated in the program IGOR (Wavemetrics) from a least-squares fit to the exponential decay and then propagating the errors through the Stern–Volmer analysis. The error in the measured N≡C cross sections was determined by a statistical analysis of the data that was collected to test whether background reaction occurred (see

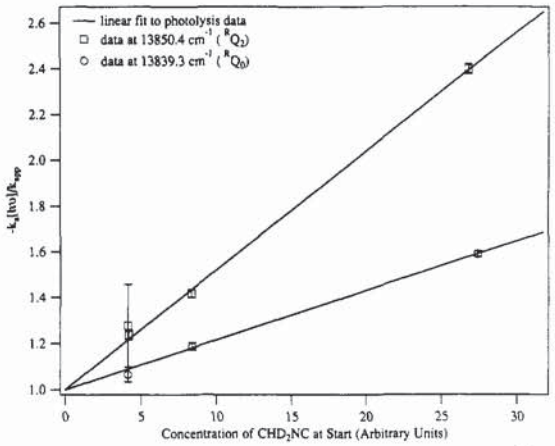

Figure 4. Reduced Stern–Volmer plot for isomerization via the $^RQ_2$ and $^RQ_0$ bandheads (see eq 3).

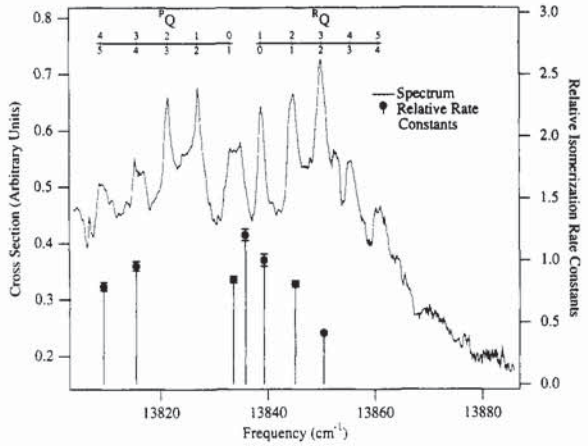

Figure 5. Expanded view of the rotationally resolved region of the CHD_2NC 5–0 C–H overtone polyad with relative overtone-induced isomerization rate constants. The height of the sticks (dot centers) represent the relative isomerization rate constants *after* correcting for the differences in absorption cross section and laser power. The error bars (hash marks on sticks) represent the 95% confidence region for each rate. These relative rate constants are normalized to the room-temperature reaction rate constant of the $^RQ_0$ ($K_{excited} = 1$) band. The numbers and hashed line above the spectrum are the spectroscopic assignments of the features. The numbers below the lines are the K quantum number before absorption of a photon, and the numbers above are the K quantum number of the excited species.

Experimental Section).[32] The error, σ, in the measured values was adjusted for the different cross sections using

$$\sigma = \sigma_0 10^{-2((g_0-g)/w)}[(10^{-2(g/w)} + 1)/(10^{-2(g_0/w)} + 1)]^{1/2} \quad (4)$$

where g is the integrated area, w is the width over which the integration was performed (136 cm^{-1}), g_0 is the average integrated area (27.241) of the spectra used to check for background reactions

(32) Walpole, R. E.; Myers, R. H. *Probability and Statistics for Engineers and Scientists*, 4th ed.; MacMillan Publishing Co.: New York, 1989.

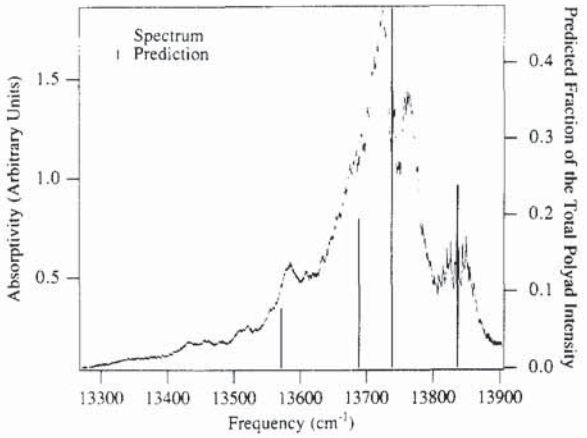

Figure 6. Photoacoustic spectrum of the CHD_2NC 5–0 C–H overtone polyad. The locations of the sticks represent the predicted band centers, and their height the predicted relative integrated intensities of the features in the polyad. They were determined by using a simple model Hamiltonian based on a Fermi resonance between the stretching and bending motions of the C–H bond.

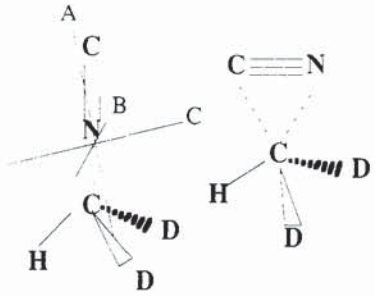

Figure 7. Geometry of CHD_2NC with approximate inertial axes (left) and the transition state (right).

(see Figure 2), and σ_0 is the statistical error (±0.066) calculated from the scatter in the background measurements. For absorbances in ln each 10 in eq 4 should be replaced by an *e*.

Another possible source of uncertainty is the error in the effective photolysis time, which is caused mostly by errors in integrating the laser power. The fractional error in this value is less than 0.001, which is a factor of 2.5 smaller than the smallest fractional error in any of the cross sections. Also, because the fitting algorithm[33] accounts for scatter in the measured decay curve caused by errors in the laser power integration, this error was neglected.

IV. Results

Figure 6 shows a room-temperature photoacoustic spectrum of the 5–0 C–H vibrational overtone transition region. Unlike the spectrum of CH_3NC, which exhibits a broad, unresolved absorption feature in this region,[19] the spectrum of CHD_2NC is structured. This structure results from two effects. First, the gross structure arises from a Fermi-resonance interaction between the stretching and bending motions of the C–H group.[34] Second, each of the bands caused by this Fermi resonance has rotational structure. The locations and lengths of the sticks in Figure 6 represent predicted band centers and relative band intensities, on the basis of assignments of the Fermi-resonance structure in the fundamentals and lower overtones.[31] A group of bands such as this is referred to as a polyad. The spectroscopy of the C–H chromophore of CHD_2NC will be discussed in detail elsewhere.[31]

The model used for predicting the location of the band centers assumes the vibrational motions of the C–H are described solely by combinations of the stretching and bending motions; the basis set used consists of the C–H stretching quantum states and the quantum states of the two C—H bends in the H—C—N≡C plane and perpendicular to it (see Figure 7). Although basis state contributions to these bands are rather complicated, the lower energy bands in Figure 6 generally have larger contributions from basis states with a large number of quanta in the bending motions of the C–H bond.[31] The largest single contribution to the high-energy band (the one used for the photolysis experiments) is the basis state that consists of four quanta in the stretch and two quanta in the in-plane bend. The contribution from five quanta in the stretching motion and no quanta in the bend is slightly more than half as large as the contribution from this bend–stretch combination state.[31]

CHD_2NC is a nearly symmetric prolate top (asymmetry parameter $\kappa \approx -0.99$). The high-energy band of the 5–0 polyad exhibits well-resolved *K* stack structure. The experiments described in this work take advantage of this assignable structure (see Figure 5). Molecules prepared via the ^PQ and ^RQ transitions become more rotationally excited in going out from the band center. The motion is not classical, but these features represent different amounts of rotational excitation about the top axis of the molecule, which lies roughly along the C—N≡C axis. Each of these features is a bandhead; thus transitions to states with varying degrees of rotational excitation about the axes perpendicular to the top axis overlap. Consequently, when a photolysis was carried out on one of the rotational features in this spectrum, the molecules were excited to a well-defined *K* rotational state (rotation about the top axis), a mixture of rotational states about the nontop axes with an average *J* value of 20, and a vibrationally excited state that corresponds to a mixture of bending and stretching motions of the C–H bond.

To test the Stern–Volmer analysis, we compared the relative absorption cross sections found using the zero-pressure intercept with the relative absorption cross sections from the photoacoustic spectroscopy (see Table II). The errors include the uncertainties in the transmission coefficient for the end mirror on the laser cavity through which the laser power was measured and the uncertainties in the intercept. Again all results are normalized to the cross section at 13839.3 cm^{-1} (the $^RQ_0$ transition). The 95%-confidence-limit errors in the cross sections from the photoacoustic measurements are believed to be approximately ±15% from previous experience.[35] The agreement shown in Table II supports the applicability of the Stern–Volmer analysis to this situation.

The relative isomerization rate constants derived from this analysis are shown in Figure 5 and listed in Table I. They are normalized to the rate constant from molecules prepared via the $^RQ_0$ transition. We do not know the absolute rate constant very accurately, but an estimate for the $^RQ_0$ transition is $k_{iso} \approx 2.7 \times 10^8\ s^{-1}$. This value assumes that $k_d \approx 1.9 \times 10^7$ Torr s^{-1}, a value derived from ref 24 by correcting for the change in reduced mass of the colliding partners. The data exhibit some noteworthy trends.

TABLE II: Comparison of the Absorption Cross Sections Generated by the Stern–Volmer Kinetics Analysis with the Cross Sections from the Photoacoustic Measurements. All Relative Cross Sections Are Normalized to the $^RQ_0$ Transition

transition	E, cm^{-1}	rel cross sections: Stern–Volmer	rel cross sections: photoacoustic	abs cross sections,[b] $\times 10^{-26}$ cm^2
$^PQ_5$	13809.3	0.59 ± 0.04	0.67 ± 0.10	0.64 ± 0.04
$^PQ_4$	13815.4	0.72 ± 0.05	0.86 ± 0.13	0.78 ± 0.05
$^PQ_1$[a]	13833.6	0.80 ± 0.05	0.81 ± 0.12	0.87 ± 0.05
^QQ[a]	13835.9	0.73 ± 0.05	0.72 ± 0.11	0.79 ± 0.05
$^RQ_0$	13839.3	1.00 ± 0.06	1.00 ± 0.15	1.09 ± 0.06
$^RQ_1$	13845.1	0.95 ± 0.06	1.12 ± 0.17	1.03 ± 0.06
$^RQ_2$	13850.4	1.39 ± 0.09	1.23 ± 0.18	1.51 ± 0.10

[a] These two bandheads overlap. The assignment is only approximate. [b] Determined from the Stern–Volmer analysis of the kinetics measurements by factoring out the mirror transmission coefficient and the cell volume.

(33) Press, W. H.; Flannery, B. P.; Teukolsky, S. A.; Vetterling, W. T. *Numerical Recipes: The Art of Scientific Computing*; Cambridge University Press: New York, 1986.

(34) Dübal, H.-R.; Quack, M. *J. Chem. Phys.* **1984**, *81*, 3779.

(35) Gutow, J. H.; Davidsson, J.; Zare, R. N. *Chem. Phys. Lett.* **1991**, *185*, 120.

TABLE III: Parameters Used for Rotational Simulations of the High-Energy Member of the CHD_2NC 5–0 C–H Polyad, Using the S Reduction. All Constants Are in Wavenumbers (cm^{-1})

	main transition		first hotband[b]		second hotband[b]	
parameter	ground state[a]	upper state	ground state	upper state	ground state	upper state
B_x	0.303 432 3	0.301 735	0.303 432 3	0.301 735	0.303 432 3	0.301 735
B_y	0.297 222 6	0.296 525	0.297 222 6	0.296 525	0.297 222 6	0.296 525
B_z	3.203 689	3.140 00	3.193 690	3.137 190	3.188 689	3.130 19
$D_J \times 10^7$	1.2415	1.383 16	1.2415	1.383 16	1.2415	1.383 16
$D_{JK} \times 10^6$	5.2942	30.0682	5.2942	30.0682	5.2942	30.0682
$D_K \times 10^5$	3.947 66	1.571 94	3.947 66	1.571 94	3.947 66	1.571 94
$d_1 \times 10^9$	−2.020 73	820.624	−2.020 73	820.624	−2.020 73	820.624
$d_2 \times 10^{10}$	−5.055 83	−1056.970	−5.055 83	−1056.970	−5.055 83	−1056.970
H_J	0.0	0.0	0.0	0.0	0.0	0.0
H_{JK}	0.0	0.0	0.0	0.0	0.0	0.0
$H_{KJ} \times 10^9$	3.82	3.82	3.82	3.82	3.82	3.82
$H_K \times 10^7$	1.12	1.12	1.12	1.12	1.12	1.12
$h_1 \times 10^{14}$	4.17	4.17	4.17	4.17	4.17	4.17
$h_2 \times 10^{14}$	2.17	2.17	2.17	2.17	2.17	2.17
h_3	0.0	0.0	0.0	0.0	0.0	0.0
ν	0.0	13 836.6	0.0	13 837.6	0.0	13 838.6

transition dipole projections (normalized to a unit vector): *A*, 0.5243; *B*, 0.6000[c]; *C*, 0.6042.

[a] From reference 57. [b] Best guess based on simulations of lower overtones, the spectra of which were taken at higher resolution. [c] The fact that a projection on the B axis is necessary to reproduce this spectrum is probably indicative of the heavy mixing of the C–H bend motions into this eigenstate because of the Fermi resonance. Only A and C projections are necessary for the lower overtones, which do not appear to be as strongly mixed.

The rate constant decreases as the final K state of the excited molecule increases. This behavior is most evident in the data from the ^RQ branch for which $\Delta K = -1$. The rate constants derived from the ^PQ branch for which $\Delta K = +1$ do not match the data from the ^RQ branch because of the overlap of the Fermi-resonance band with the lower energy with the ^PQ branch. The isomerization rate constant increases at higher temperatures for all the transitions studied at 50 °C, but the enhancement is less than 47%.

No data are presented for the $^PQ_3$ transition. We did attempt to collect such data but could not obtain reproducible results. One possible explanation is that the bandhead has some sharp transitions we were unable to see in our spectra. Our multimode laser may be hopping on and off these transitions. This band deserves study at higher resolution.

V. RRKM Simulations

The rate constant for each J,K state was calculated using the RRKM formalism. In RRKM theory the reaction rate constant, $k(E)$, for a molecule with an amount E of internal energy is given by

$$k(E) = W^{\dagger}(E - E_0)/h\rho(E) \qquad (5)$$

where $\rho(E)$ is the density of quantum states in the reactant at energy E, $W^{\dagger}(E - E_0)$ is the sum of states available in the transition state with energies between zero and $E - E_0$, and h is Planck's constant. This equation is the standard RRKM expression for the rate constant. In this study the sums and densities of states were calculated using the Beyer–Swinehart algorithm.[2-4]

To calculate the relative rate constants using the RRKM formalism, we must know the rotational distribution of excited molecules. We approximated this distribution by calculating the absorption spectrum for the C–H chromophore of CHD_2NC in the photolysis region using a computer program by Luckhaus and Quack[36] for simulating vibrational spectra of asymmetric rotors. The simulation included relative contributions of 0.59 and 0.26, respectively, from the first and second hotbands of the two nearly degenerate C—N≡C bending modes (253 cm^{-1}). The parameters used for the simulation were determined by fitting the parameters for the lower overtones and using the variation of these to predict the parameters for the 5–0 overtone.[31] The simulation spectrum is shown in Figure 8, and the parameters are shown used in Table III. The simulation provides a reasonable prediction of the distribution of rotational states from which a laser-excited population can react.

(36) Luckhaus, D.; Quack, M. *J. Chem. Phys.* **1989**, *68*, 745.

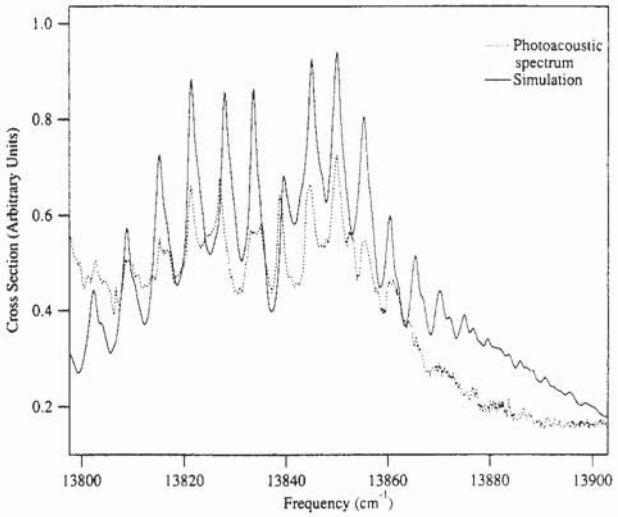

Figure 8. Simulation (solid line) and real spectrum (dashed line) of the highest energy member of the CHD_2NC 5–0 C–H overtone polyad.

The RRKM rate constants for a specific laser excitation frequency were calculated by taking the weighted average of the RRKM rate constants for each of the J,K states excited by the laser. The weighting was calculated as the product of the relative excited population and the relative laser intensity versus frequency. The laser profile was assumed to be a 0.5 cm^{-1} fwhm Gaussian. We ignored transitions sufficiently far from the laser center frequency that the laser intensity was a factor of less than 10^{-4} that of the peak intensity.

Figure 9B is a graphic representation of the reaction coordinate. The barrier height (E_0) used was 13 237.3 cm^{-1} (37.85 kcal/mol), as suggested by Rabinovitch's thermal studies.[12-15] The vibrational energy ($\approx E$) of the reactant was assumed to be 13 836.6 cm^{-1} (39.56 kcal/mol), the band center of the vibrational overtone transition. Table IV lists the parameters used for the RRKM calculations. Rate constants for reaction from states arising from hotband transitions were calculated by adding 253 cm^{-1} (frequency of the lowest energy mode in the molecule) of energy to the vibrational energy for the first hotband and twice that for the second hotband.

Equation 5 shows that the rate constant for an energized molecule depends upon the height of the barrier to reaction, E_0, and the amount of energy in the molecule, E. An increase in the barrier height, E_0, decreases the value of the reaction rate constant

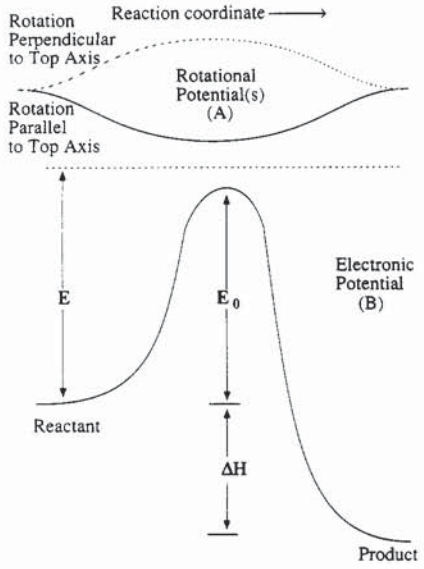

Figure 9. Representation of the potential energy along the reaction coordinate for the CHD_2NC isomerization. The two curves in A are the potentials caused by rotation. The curve in B is the electronic potential.

TABLE IV: Parameters Used for the RRKM Calculations

	vibrational frequencies cm^{-1}		I, uÅ^2	
assignment	reactant[a]	transition state[b]	reactant[a]	transition state[b]
C—D stretch	2194.1	2194.1		
N≡C stretch	2163.9	1970.0	5.27 (I_a)	13.58 (I_a)
CD_2 scissor	1084.2	1084.2		
C—N stretch	984.3	609.0		
C—H stretch	2988.9	2988.9		
C—H bend	1331.0	1331.0	55.56 (I_b)	38.60 (I_b)
CD_2 wag	882.1	700.0		
C—D stretch	2254.0	2254.0		
C—H bend	1293.0	1293.0		
CD_2 rock	900.0	700.0	56.72 (I_c)	45.76 (I_c)
C—N—C bend	253.0	230.0		
C—N—C bend	253.0			

Vibrational Energy = 13 836.6 cm^{-1} (39.56 kcal/mol)
E_0 = 13 237.3 cm^{-1} (37.85 kcal/mol)
Laser Bandwidth = 0.5 cm^{-1}

[a] From reference 58. [b] Based on ref 17. Motions involving the D atoms were shifted down to account for the increase in mass as compared with H. Geometry was recalculated assuming the C–D bond length is approximately 0.002 Å shorter than that of the C–H.[57]

because the range over which the quantum states of the transition state are summed decreases, thereby reducing $W^\dagger(E - E_0)$. Likewise, putting more energy into the molecule increases E and probably increases the value of $k(E)$. The reaction rate constant for a rotating molecule depends upon how $W^\dagger(E - E_0)$ and $\rho(E)$ change with rotational state.

Because the CHD_2NC molecule is a nearly symmetric prolate top, it can undergo two kinds of rotational motion: rotation about the top axis, A in Figure 7, or rotation about an axis perpendicular to the top axis, for example, B in Figure 7. The rotational states can be specified by two quantum numbers, J and K, where the quantum mechanical rotational energy in wavenumbers (cm^{-1}) of the system is

$$E_{rot} = \frac{\hbar}{4\pi c}\left[\frac{J(J+1)}{I_\perp} + \left(\frac{1}{I_A} - \frac{1}{I_\perp}\right)K^2\right] \qquad (6)$$

Here J is the total angular momentum, K is the projection of the angular momentum on A (the top axis, see Figure 7), $I_{A,B,orC}$ are the moments of inertia of the molecule, $I_\perp$ is the average of I_B and I_C, and c is the speed of light. K is constrained to be less than or equal to J. Molecules in high K states are rotating faster about the top axis, and the higher the J value for a given K the faster they are rotating about an axis perpendicular to the top axis. For low quantum states, the motion is not classical and thus the above picture is a simplification, but it is adequate for our purposes.

Consider two cases: first, where the K quantum number is not conserved throughout the reaction and second, where K is conserved. The total angular momentum, J, must be conserved for any isolated molecule, so the effect of J excitation is analogous to the second case.

If K is not conserved throughout the reaction, then any energy associated with the K quantum number is available for reaction; thus $E = E_{vib} + E_K$, where E is the total energy available for reaction, E_{vib} is the vibrational energy, and $E_K = K^2/I_A$ is the energy associated with the K quantum number. Assuming E_K is available for reaction implies that energy is freely exchanged between states with the same J, namely, rotational states of different K and vibrational states; therefore, the K quantum states also contribute to the bath of states throughout which energy is randomized. The extra bath states are accounted for by including K quantum states in the sum of states, $W^\dagger(E - E_0)$, and the density of states, $\rho(E)$ (see eq 5). In the calculations carried out in this study and in most other RRKM analyses, the number and distribution of contributing rotational states are calculated classically. Rotation associated with K is treated by assuming that the available states are the states of a classical one-dimensional rotor with a moment of inertia equal to the moment of inertia about the top axis.[2,3] Since E grows as K increases, the reaction rate constant should increase as K grows. This conclusion assumes that the variation of $W^\dagger(E - E_0)$ and $\rho(E)$ with E is sufficiently smooth so that the ratio given by eq 5 varies monotonically with E.[37] This assumption is expected to hold because of the presence of low-frequency modes in the transition state.

Implications of this model (J conserved/K active) are discussed in greater detail by Zhu and Hase.[38] We use this model for most of the RRKM calculations done in this study. Recent experimental work[39] suggests that this treatment is reasonable at the high energies reached in our experiment (roughly equivalent to the average energy of a Boltzmann distribution of CHD_2NC molecules at 1500 K).

If the quantum number K is conserved throughout the reaction, then the picture is somewhat more complicated. E_K is not directly available for reaction, and the rotational states are not coupled to the bath states. The effect of rotation, which results now solely from angular momentum conservation, is most easily treated as a modification of the potential surface upon which the reaction takes place. In this simple case of isomerization with a large barrier to reaction, the result is simply to shift the height of the barrier to reaction.[2,3] In eq 5, E_0 is replaced by $E_{eff} = E_0 + V_0(K)$.

Classically, if a molecule rotates about its top axis A (see Figure 7) with some angular momentum, l, the energy required is

$$E_{rot} = l^2/I_A \qquad (7)$$

where I_A is the moment of inertia about the top axis. As the N≡C group rotates toward the transition state (see Figure 7), the moment of inertia, I_A, increases (see Table IV). Equation 7 shows that if l is conserved E_{rot} decreases. In the case of a symmetric top such as CHD_2NC, $\Delta E_{rot} = K^2(1/I_A^T - 1/I_A^R)$, where K is the initial reactant rotational quantum number, I_A^T is the moment of inertia about the top axis in the transition state, and I_A^R is the moment of inertia for the reactant. The extra energy goes into increasing the rate of rotation of the N≡C group. Since angular momentum must be conserved, all the energy cannot go into the rotation of the N≡C group; some of it must cause the whole molecule to rotate in the opposite direction. Because the molecule is large compared with the N≡C group, this energy is a small fraction of the total. The net effect is to generate a centrifugal or rotational potential, as shown in Figure 9A, making the

(37) King, K. D.; Nguyen, T. T.; Gilbert, R. G. *J. Chem. Phys.* **1981**, *61*, 221.
(38) Zhu, L.; Hase, W. L. *Chem. Phys. Lett.* **1990**, *175*, 117.
(39) Farley, F. W.; Novakoski, L. V.; Dubey, M. K.; Nathanson, G. M.; McClelland, G. M. *J. Chem. Phys.* **1988**, *88*, 1460.

TABLE V: Rate Constants Calculated Using the RRKM Formalism As Described in the Text. Note These Constants Are the Calculated Constants Multiplied by a Factor of 3 To Account for the Reaction Path Degeneracies

final K	transition	E, cm^{-1}	calculated rate, 10^8 s^{-1} without hotbands	calculated rate, 10^8 s^{-1} with hotbands[a]
4	$^PQ_5$	13809.3	0.980	1.33
3	$^PQ_4$	13815.4	0.934	1.23
0	$^PQ_1$	13833.6	0.897	1.40
?	^QQ	13835.9	0.930	1.39
1	$^RQ_0$	13839.3	0.977	1.39
2	$^RQ_1$	13845.1	0.935	1.41
3	$^RQ_2$	13850.4	0.936	1.34

[a] This is the weighted average of the rates calculated for the normal transition and the first and second hotband transitions. The weights were 1.0:0.59:0.26.

transition state the preferred geometry in the absence of other potential terms. If we assume, as we believe is justified, that the rotational potential is much broader than the electronic potential (see Figure 9), the sum of these two potentials would lower the barrier height, i.e., $V_0(K) = K^2(1/I_A^T - 1/I_A^R)$ is negative. Again the net effect is to increase the reaction rate constant. A similar argument shows that rotation about an axis perpendicular to the top axis has the opposite effect. Hence, for a given K state the reaction rate constant decreases as J increases. We did perform some calculations assuming that both K and J were conserved. The calculated rate constants were about 25% larger than those with K not conserved, but the basic trends did not change. The observed variation in the rate constant is about a factor of 2 larger than the difference between calculations in which K is and is not conserved.

We conclude that an increase in K is expected to accelerate the reaction independent of whether or not K is conserved, whereas an increase in J is expected to slow the reaction. The interaction of these two effects can be seen by comparing the average J contributions at each photolysis frequency, listed in Table VI, with the calculated isomerization rates (Table V and Figure 10). Sources of error include estimates from ab initio calculations[17] of the transition-state frequencies and geometries, use of ground-state rotational constants even at high energies, and errors in the spectroscopic simulation used to predict which J,K states were excited. Since our spectroscopic simulation is only a "best guess", these calculations should not be construed as a strict test of the assumptions used in RRKM theories, although the calculations are certainly among the more demanding tests to date.

If contributions from the hotband transitions are not included, the model (J conserved/K active) predicts that the rate constant should increase as a higher final K state is accessed on the P ($\Delta K = -1$) side of the spectrum. When the hotbands are included, the model predicts a *decrease* in the rate constant with an *increase* in K. Note, however, that the $^RQ_1$ transition is not predicted to follow this trend when hotbands are included. Otherwise, these calculations reproduce the direction of the experimental trends but not the magnitudes of the changes.

Although the spectroscopic simulation used to determine the excited distribution is inexact, we believe that the discrepancies between experiment and theory are significant. We tried varying

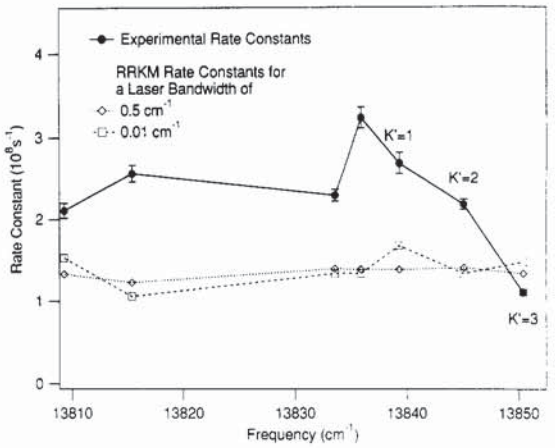

Figure 10. Comparison of RRKM calculations (K not conserved) with experimental results. If K is conserved in the calculations, the rate constants are about 25% higher. The lines are provided to guide the eye. The experimental $K' = 1$, 2, and 3 rate constants derived from the ^RQ brands are indicated.

the laser bandwidth used for excitation in the calculations. This variation dramatically changed the assumed excited distribution. Nevertheless, we saw variations in the rate constant of more than a few percent only when the bandwidth was decreased by a factor of 50 to a bandwidth of 0.01 cm^{-1} (see Figure 10)! At this small bandwidth, we no longer observed any trend in the rate constant with a change in K and did see fluctuations in the predicted rate constants of as much as 37%. These variations are somewhat smaller than those observed experimentally. The bandwidth of 0.01 cm^{-1} is the minimum spectroscopic bandwidth possible for a 6-Torr sample of this molecule on the basis of the pressure broadening of approximately 1 cm^{-1}/atm observed in high-resolution fundamental spectra.[31] At this narrow bandwidth, only 5–21 transitions contribute to the excited-state population. These calculations suggest that even significant variation of the excited distribution (major errors in the simulation) is unlikely to account for the discrepancy between calculations and experimental data. Additionally, none of the Stern–Volmer plots produced by this experiment exhibited any curvature; this suggests that a spread in reaction rate constants does not appreciably contribute to the average rate constant. We also raised the barrier height stepwise until it was equal to the vibrational energy of the reactant. The only significant effect of this variation was to reduce the calculated rate constants. The variation of isomerization rate constant with rotation changed little. Apparently, some important effect is overlooked in the standard RRKM theory. We suggest that this problem concerns the way in which angular momentum couples to the reaction coordinate. The simple limiting approximations made in what we call standard RRKM theory are inadequate to account for isomerization rate constants at this level of detail.

VI. Discussion

The present experiments demonstrate that the initial rotational state of the reactant, CHD_2NC, has a significant effect upon the isomerization rate constant (see Figure 5 and Table I). Specifically, *increasing* the K quantum number *decreases* the isomerization rate constant, even within the very small range of K values

TABLE VI: Weighted Average and Standard Deviation (in Parentheses) of the J States Excited at Each Photolysis Frequency. The Intensity Versus Frequency Profile of the Laser Was Approximated as a 0.5 cm^{-1} Fwhm Gaussian

final K	transition	E, cm^{-1}	$\langle J\rangle_{main}$	$\langle J\rangle_{hotband1}$	$\langle J\rangle_{hotband2}$	$\langle J\rangle_{av}$[a]
4	$^PQ_5$	13809.3	17.7 (10.8)	28.8 (7.8)	32.7 (10.8)	23.4 (8.0)
3	$^PQ_4$	13815.4	18.2 (8.9)	30.1 (7.8)	27.2 (12.9)	23.3 (6.7)
0	$^PQ_1$	13833.6	16.4 (8.5)	19.8 (10.9)	19.3 (11.9)	17.9 (6.1)
?	^QQ	13835.9	17.8 (12.3)	17.9 (11.9)	16.7 (8.8)	17.7 (7.7)
1	$^RQ_0$	13839.3	12.3 (8.2)	19.0 (9.2)	23.3 (9.6)	16.0 (6.3)
2	$^RQ_1$	13845.1	17.5 (9.3)	18.8 (8.2)	22.2 (10.8)	18.6 (6.1)
3	$^RQ_2$	13850.4	17.0 (9.5)	25.8 (6.4)	26.5 (9.9)	21.1 (6.7)

[a] This is the weighted average of the contributions from the three transitions ($\langle J\rangle_{main} + 0.59\langle J\rangle_{hotband1} + 0.26\langle J\rangle_{hotband2}$). The standard deviation of this value should be used only as a guide because it is calculated assuming the other averages are randomly distributed, which they are not.

experimentally accessed (0–4). We have attempted to simulate the isomerization rate constants using a standard implementation of RRKM theory that includes the effects of rotation (see Figure 10 and Tables IV and V). Simulations using only one kind of angular momentum coupling are unable to reproduce the experimental results.

We have explored two extreme cases of angular momentum conservation, one in which K is conserved and the other in which K is not conserved. We find that the calculated rate constants increase by about 25% when K is conserved, whereas the maximum variation we observed is about 50%. This finding suggests to us the possibility that the degree of K conservation may be J,K dependent.[40] Such behavior, if true, requires that the extent of angular momentum coupling be known a priori before RRKM simulations can be applied correctly. This level of understanding is currently not available; we expect that experiments at the level of detail of those described here may teach us how to deal with such phenomena.

Although we believe that detailed angular momentum coupling is responsible for the observed experimental variation in the isomerization rate constants, other possibilities cannot be completely discounted:

(1) The variation in rate constants could be caused by hotband transitions. Our data suggest that this effect is implausible because the fractional change in the rate constant upon heating the sample for the $^RQ_0$ transition is 0.41 versus a fractional change of 0.47 for the $^RQ_1$ transition (see Table I). The larger fractional change for the smaller rate constant is inconsistent with the concept that hotbands account for the difference in rate constants. If a rate constant is larger because of contributions from a hotband, then as the temperature increases the rate constant should increase faster than a rate constant that has less contribution from a hotband. From spectroscopic simulations, hotbands are expected to make roughly similar contributions to each bandhead.

(2) The electronic potential could be much broader than we think, so that the sum of the electronic and rotational potentials creates a small well at the top of the barrier instead of just lowering the barrier (see Figure 9). This effect would allow "rotational trapping" of the transition state. Because the experiment is done only about 1.7 kcal/mol above the barrier, a small well would make a large difference in the observed reaction rate constants. This pathological behavior seems unlikely but cannot be ruled out.

(3) The trend in rate constants could be caused by rotational-state-dependent deactivation of the excited molecules, in other words, the dependence of k_d on K (see Data Analysis). Trajectory calculations on SO_2–Ar collisions and HO_2–He suggest, however, that vibrational energy transfer is not highly dependent upon the rotational state of the molecule.[41-43] Also, recent work on D_2CO vibrational and rotational energy-transfers indicates that the rotational populations would be completely scrambled before vibrational energy transfer is likely to occur.[44,45] To test the sensitivity of the deactivation to rotational state, we repeated the isomerization study using Ar as a buffer gas. The measurements yielded very high uncertainty because of the large dilution factor necessary to ensure that the excited CHD_2NC molecules collided mostly with Ar, but the variation in relative rate constants versus rotational state appeared close to that of the neat case. This result suggests that the observed rotational dependence is not caused by rotational-state-dependent vibrational energy transfer. The proper test of this supposition would be to compare these experimental results with those from an experiment without collisional deactivation. Unfortunately, such a test would be extremely difficult because of the weakness of the overtone transitions and thus the small number of excited molecules produced. If rotational-state-dependent collisional deactivation is the explanation, then unimolecular reaction rate theories must be amended; such behavior would affect both the activation and deactivation steps in thermal experiments.

There is a paucity of other experimental work bearing on the importance of rotational effects in unimolecular decomposition.[46-56] Perhaps most germane to the present study are the real-time experiments by Zewail and co-workers on the unimolecular reactions $NCNO \rightarrow CN + NO$[50] and $H_2O_2 \rightarrow 2OH$.[55] In both cases quasi-biexponential behavior is observed in the buildup of the photofragment. Zewail and co-workers suggest that non-RRKM behavior associated with noncommunicating portions of phase space reflecting the dissociation of molecules with different J,K states explains this time dependence. Once again, the lack of definition of the J,K states prepared, however, makes further analysis problematic.

VII. Conclusions

Although the effects of angular momentum coupling are known for the rates of unimolecular dissociation, this work represents the first observation of a rotational-state dependence for the rates of unimolecular isomerization. The results indicate the reality of rotational effects and, therefore, the importance of including them correctly in calculations of reaction rate constants. The thermal and overtone-induced isomerizations of CH_3NC to CH_3CN is a system well known to follow the predictions of RRKM theory. It comes as no surprise then to find that the overtone-induced isomerization of CHD_2NC to CHD_2CN is also well characterized by the basic assumption of RRKM theory, namely, rapid energy randomization. This belief is supported by the fact that the RRKM rate constants fall within the range of rate constants observed experimentally. Here the RRKM calculations use the following information. The vibrational frequencies and moments of inertia were determined spectroscopically and from ab initio calculations, the height of the barrier to reaction was determined independently in previous thermal studies, and the excited distribution was based on the observed spectra and measured laser bandwidth profile. Nevertheless, at the level of detail in which contributions from small numbers of individual J,K states are apparent, we find significant discrepancies between our experimental isomerization rate constants and those calculated from standard RRKM theory in which angular momentum effects are included assuming one of two extremes, either K conservation or K nonconservation in the transition state. The variation between these extreme cases is about 50% of that observed experimentally. We tentatively suggest that variation in the extent of K conservation with J,K state might account for a major portion of the observed variation in isomerization rate constant with laser wavelength. To test this possible explanation, however, further knowledge of the J and K distribution in the CHD_2NC overtone

(40) Lawrance and Knight (Lawrance, W. D.; Knight, A. E. W. *J. Phys. Chem.* **1988**, *92*, 5900) have carefully examined the rotational-state dependence of Coriolis and centrifugal coupling, and it might be expected from their work that the change in coupling strength is not strongly dependent on J and K. This conclusion, however, may not apply to the transition state.

(41) Schranz, H. W.; Troe, J. *J. Phys. Chem.* **1986**, *90*, 6168.
(42) Hippler, H.; Schranz, H. W.; Troe, J. *J. Phys. Chem.* **1986**, *90*, 6158.
(43) Brown, N. J.; Miller, J. A. *J. Chem. Phys.* **1984**, *80*, 5568.
(44) Bewick, C. P.; Martins, J. F.; Orr, B. J. *J. Chem. Phys.* **1990**, *93*, 8643.
(45) Bewick, C. P.; Orr, B. J. *J. Chem. Phys.* **1990**, *99*, 8634.
(46) Neusser, H. J. *J. Phys. Chem.* **1989**, *93*, 3897.
(47) Kiermeier, A.; Kühlewind, H.; Neusser, H. J.; Schlag, E. W. *J. Chem. Phys.* **1988**, *88*, 6182.
(48) Polik, W. F.; Guyer, D. R.; Moore, C. B. *J. Chem. Phys.* **1990**, *92*, 3453.
(49) Foy, B. R.; Casassa, M. P.; Stephenson, J. C.; King, D. S. *J. Chem. Phys.* **1989**, *90*, 7037.
(50) Foy, B. R.; Casassa, M. P.; Stephenson, J. C.; King, D. S. *J. Chem. Phys.* **1990**, *92*, 2782.
(51) Khundkar, L. R.; Knee, J. L.; Zewail, A. H. *J. Chem. Phys.* **1987**, *87*, 77.
(52) van Koppen, P. A. M.; Brodbelt-Lustig, J.; Bowers, M. T.; Dearden, D. V.; Beauchamp, J. L.; Fisher, E. R.; Armentrout, P. B. *J. Am. Chem. Soc.* **1990**, *112*, 5663.
(53) Viggiano, A. A.; Morris, R. A.; Dale, F.; Paulson, J. F.; Giles, K.; Smith, D.; Su, T. *J. Chem. Phys.* **1990**, *93*, 1149.
(54) Meisels, G. G.; Verboom, G. M. L.; Weiss, M. J.; Hsieh, T. *J. Am. Chem. Soc.* **1979**, *101*, 7189.
(55) Luo, X.; Rizzo, T. R. *J. Chem. Phys.* **1991**, *94*, 889.
(56) Scherer, N. F.; Zewail, A. H. *J. Chem. Phys.* **1987**, *87*, 97.
(57) Halonen, L.; Mills, I. M. *J. Mol. Spectrosc.* **1978**, *73*, 494.
(58) McKean, D. C.; Duncan, J. L.; MacKenzie, M. W. *J. Mol. Spectrosc.* **1977**, *42*, 77.

spectrum will be required; conversely, such detailed studies, as started here, should test our present understanding of unimolecular isomerization and reveal the importance of rotation-induced intramolecular couplings in how unimolecular processes occur.

Acknowledgment. We thank David Klenerman for suggesting that CHD_2NC might be an interesting system to study because of the Fermi-resonance interaction. We would also like to thank Kieran Lim, Brian Wladkowski, Jennifer Mihalick, and John Brauman for helpful discussions. Additionally, Jennifer Mihalick provided us with computer code for the Beyer–Swinehart-state counting algorithm including rotations. We would also like to thank one of our reviewers for carefully checking our paper and pointing out minor mistakes. This research was supported by the U.S. National Science Foundation under Grants NSF CHE 89-21198 and NSF CHE 90-07939.

$F_2 + CF_3I$ Dark Reaction. 1. Stoichiometry and Pressure-Dependent Kinetics

D. E. Johnson,† J. C. Whitehead,‡ E. A. Walters,† and E. A. Dorko*

Lasers and Imaging Directorate (PL/LIDB), Phillips Laboratory, Kirtland AFB, Albuquerque, New Mexico 87117 *(Received: August 19, 1991; In Final Form: November 19, 1991)*

The reaction between F_2 and CF_3I has been investigated over a wide range of pressures and flow velocities at 298 K. An induction time precedes a period of CF_3I consumption which is well characterized by an exponential decrease in concentration over time. The CF_3I disappearance rate as well as the induction time are dependent upon the concentration of the initial species, indicating that a chain reaction is responsible. CF_3I and F_2 react to give IF_5, C_2F_6, and CF_4 as end products (where the principal carbon-containing end product is CF_4), suggesting that both IF and CF_3 play an important role in the kinetics of the reaction. The apparent discrepancies of the previous studies of this reaction are shown to be related to experimental conditions.

Introduction

Iodine monofluoride has received much attention recently because of its potential as a lasant in a visible chemical laser. Lasing from the $B \rightarrow X$ transition through optical pumping was demonstrated by Davis and co-workers,[1,2] who found the $B^3\Pi(0^+)$ state to be very stable. This work was extended by Whitefield et al.,[3] who produced significant quantities of IF(B) through collisional pumping of the ground state with $O_2(^1\Delta)$. The potential of $O_2(^1\Delta)$ as a chemical pump source for a $B \rightarrow X$ laser has been reviewed by Whitefield[4] and continues to be the focus of work.[5,6] Other chemical pump sources for IF(X) have been investigated as well. $N_2(A^3\Sigma_u^+)$ metastables have been used to generate IF(B),[7,8] and the role of $NF(a^1\Delta)$ and $NF(b^1\Sigma^+)$ in the production of IF(B) has also been examined.[9,10]

Experiments utilizing the alkyl iodides have played an important role in understanding how IF(B) can be formed. Indeed, Zolotarev and co-workers have produced lasing from the IF(B) state by the optical excitation of IF(X) which was formed following the photolysis of $CF_3I/NF_2/He$ mixtures.[11,12] In a series of experiments by Raybone et al., various iodides were mixed with F atoms to yield IF(B) emission which was considerably enhanced by adding $O_2(^1\Delta)$ to the reaction flame.[13,14] The same group has also produced IF(B) emission by 248-nm photolysis of alkyl iodide/F_2 mixtures.[15,16] From the results of these studies[13-16] it has been suggested that IF(B) is formed either by the recombination of $I^*(^2P_{1/2})$ and F atoms or by sequential excitation of IF(X) by I^*. A definitive interpretation has been precluded by a lack of understanding of F_2/alkyl iodide dark reaction kinetics, although Davis and Woodward have recently established the steps by which $O_2(^1\Delta)$ sequentially pumps IF(X) to IF(B).[6]

Some cursory studies of the reaction between F_2 and the alkyl iodides have been made. Estler et al.[17] reported $IF(B \rightarrow X)$ emission from the high-pressure reactions $F_2 + CH_3I$, CF_3I, CH_2I_2, and HI. Burrows[18] reported that the alkyl iodides CF_3I, $i\text{-}C_3F_7I$, and $n\text{-}C_3F_7I$ reacted with F_2 so that the alkyl iodide was completely consumed whenever $[F_2] \geq 3[RI]$, where RI represents the alkyl iodide. From this result he postulated a global reaction of the form

$$RI + 3F_2 \rightarrow RF + IF_5 \quad (1)$$

Berman and Whitefield[19] reported evidence of a chain reaction between F_2 and CF_3I, and suggested that the initiation step was

$$CF_3I + F_2 \rightarrow CF_3IF + F \quad (2)$$

in analogy with the initiation step of the $CH_3I + F_2$ system.[20] On

† Department of Chemistry, University of New Mexico, Albuquerque, NM 87131.
‡ Department of Chemistry, University of Manchester, Oxford Road, Manchester, M13 9PL, United Kingdom.

(1) Davis, S. J.; Hanko, L.; Shea, R. F. *J. Chem. Phys.* **1983**, *78*, 172.
(2) Davis, S. J.; Hanko, L.; Wolf, P. J. *J. Chem. Phys.* **1985**, *82*, 4831.
(3) Whitefield, P. D.; Shea, R. F.; Davis, S. J. *J. Chem. Phys.* **1983**, *78*, 6793.
(4) Whitefield, P. D. *J. Photochem.* **1984**, *25*, 465.
(5) Helms, C. A.; Hanko, L.; Healey, K.; Hager, G.; Perram, G. P. *J. Appl. Phys.* **1989**, *66*, 6093.
(6) Davis, S. J.; Woodward, A. M. *J. Phys. Chem.* **1991**, *95*, 4610.
(7) Piper, L. G.; Marinelli, W. J.; Rawlins, W. T.; Green, B. D. *J. Chem. Phys.* **1985**, *83*, 5602.
(8) David, S. J.; Ongstad, A. P.; MacDonald, M. A.; Coombe, R. D. *Chem. Phys. Lett.* **1987**, *136*, 352.
(9) Pritt, A. T., Jr.; Patel, D.; Benard, D. J. *Chem. Phys. Lett.* **1983**, *97*, 471.
(10) Zhuang, Q.; Huang, R.; Sang, F.; Cui, T.; Yuan, Q.; Zhang, C. *Chin. Phys.—Lasers* **1988**, *15*, 6.
(11) Zolotarev, V. A.; Kryukov, P. G.; Podmar'kov, Yu. P.; Frolov, M. P.; Shcheglov, V. A. *Sov. J. Quantum Electron.* **1988**, *18*, 643.
(12) Zolotarev, V. A.; Kryukov, P. G.; Podmar'kov, Yu. P.; Frolov, M. P.; Shcheglov, V. A. *Sov. J. Quantum Electr.* **1988**, *18*, 1464.
(13) Raybone, D.; Watkinson, T. M.; Whitehead, J. C. *Chem. Phys. Lett.* **1987**, *135*, 170.
(14) Raybone, D.; Watkinson, T. M.; Whitehead, J. C. *J. Chem. Soc., Faraday Trans. 2* **1987**, *83*, 767 and references therein.
(15) Raybone, D.; Watkinson, T. M.; Whitehead, J. C. *Chem. Phys. Lett.* **1987**, *139*, 442.
(16) Raybone, D.; Watkinson, T. M.; Whitehead, J. C.; Winterbottom, F. *Laser Chem.* **1988**, *9*, 369.
(17) Estler, R. C.; Lubman, D.; Zare, R. N. *Faraday Discuss. Chem. Soc.* **1977**, *62*, 317.
(18) Burrows, M. D. *J. Chem. Phys.* **1984**, *81*, 3546.
(19) Berman, M. R.; Whitefield, P. D. *J. Chem. Phys.* **1986**, *84*, 4281.